Computers and Geosciences 122 (2019) 15–24

Contents lists available at ScienceDirect

Computers and Geosciences

journal homepage: www.elsevier.com/locate/cageo

A closed-form solution for the horizontally aligned thermal-porous spheroidal inclusion in a half-space and its applications in geothermal reservoirs

Xiangning Zhang[a], Ding Lyu[a], Pu Li[a], Xiaoqing Jin[a,b,*,1], Peter K. Liaw[c], Leon M. Keer[d]

[a] State Key Laboratory of Mechanical Transmissions, Chongqing University, Chongqing, 400030, China
[b] College of Aerospace Engineering, Chongqing University, Chongqing, 400030, China
[c] Department of Materials Science and Engineering, University of Tennessee, Knoxville, TN, 37996, USA
[d] Department of Mechanical Engineering, Northwestern University, Evanston, IL, 60208, USA

ARTICLE INFO

Keywords:
Spheroidal inclusion
Thermo-porous eigenstrains
Semi-infinite space
Geophysics
Geothermal reservoirs

ABSTRACT

The inclusion model for pore pressure and near surface localized heating may be of practical importance to many geological applications including geothermal reservoirs and volcanoes. In literature, the axisymmetric inclusion problems considering *vertically* placed spheroidal inclusions have been examined, while the complementary problems concerning *horizontal* spheroidal inclusion have not drawn much attention. The latter lacks axial symmetry, and usually cannot be handled by the analytical methods developed for the symmetric case. The current work analytically explores this *asymmetric* problem of thermo-porous spheroidal inclusion with the assistance of geometric interpretation. The complete solution to the displacement, strain and stress is formulated in Cartesian coordinates for ease of engineering applications. The formulae are derived in compact closed-form expressions in terms of elementary functions, which are handy for analytical manipulations and computer programming. Furthermore, applications in geostructures are discussed, and benchmark examples are provided to validate the present solution.

1. Introduction

Eshelby's celebrated works (Eshelby, 1957, 1959), have helped shape many fields of modern science and technology over the past decades. Particularly in geophysical engineering, the Eshelby inclusion model has been considered as an effective tool in dealing with many related problems including geostructures, caverns and geothermal reservoirs (Rudnicki, 2011; Bedayat and Dahi Taleghani, 2015; Im et al., 2017). Although it might be more realistic and necessary to adopt a half-space model when the geothermal structures are located in shallow ground, most studies (e.g., Healy, 2009; Meng et al., 2012) focus on the inclusions in a full-space. This is presumably because the analytical studies of the half-space inclusion problem are intricate and the available solutions are limited. Mindlin and Cheng (1950) solved the spherical inclusion with uniform dilatational thermal expansion by utilizing the Galerkin vector stress function. Chiu (1978) formulated the analytical solution of uniformly distributed cuboidal inclusion by employing the method of images. Chiu's work (1978) was refined later by Liu et al. (2012), where an ingenious application of the Fast Fourier Transform technique is proposed for numerical computation of the half-space inclusion problem. Seo and Mura (1979) investigated the elastic field of a semi-infinite space containing an ellipsoidal inclusion with pure dilatational eigenstrain. Although Seo and Mura did not present the final formulae in explicit form, they plotted the stress results corresponding to the axisymmetric case when the inclusion is a spheroid. Recently, Seo and Mura's problem was revisited by Lyu et al. (2018) where the complete elastic field solutions were given analytically in explicit form. Two major complexities, due to the cubic root and involved elliptic functions, are unavoidable in the analytical representation (Lyu et al., 2018), leading to the limited manageability of their solutions.

In the case of dilatational eigenstrains, the deformation tendency of the inclusion would be to expand isotropically, as would be the case for poroelastic or thermoelastic strains in an isotropic medium (Soltanzadeh and Hawkes, 2008). Accordingly, the thermo-porous

* Corresponding author. State Key Laboratory of Mechanical Transmissions, Chongqing University, Chongqing, 400030, China.
E-mail address: jinxq@cqu.edu.cn (X. Jin).

[1] X. Z. and X. J. designed research and wrote the paper; X. Z. and D. L. performed analytical derivation and verification; P. L. helped explore the numerical examples through programming; X. J. provided theoretical and technical guidance for all aspects of the project; P. K. L. and L. M. K. revised the manuscript and supervised the study.

https://doi.org/10.1016/j.cageo.2018.10.001
Received 16 July 2018; Accepted 1 October 2018
Available online 09 October 2018
0098-3004/

Nomenclature

a	The radius of spherical inclusion
a_I	Semi-axis of the ellipsoidal inclusion
c	Depth location of the ellipsoid center
E	Young's modulus
H	Symbols to simplify the expression
n_i , n_i^*	Outward unit normal vector
P, P_0	Pore pressure and unstrained state of pore pressure
Q_{ij}	Symbols to simplify the expression
S_{ij}, s_{ij}	Strain influence coefficients for the exterior and interior field
T_{ij}, t_{ij}	Stress influence coefficients for the exterior and interior field
T, T_0	Temperature and unstrained state of temperature
W_i, w_i	Displacement influence coefficients for the exterior and interior field
$u_i(\mathbf{x})$	Displacement components
x_1, x_2, x_3	Coordinate system
$\mathbf{x}$	A target field point of the elastic space
α	The ratio of a_1 to a_3
α_B	Biot pore-pressure coefficient
β, γ	Symbols to simplify the expression
Δ	Denotes the "jump" of elastic components
ΔT, ΔP	Changes of temperature and pore pressure
$\varepsilon_{ij}(\mathbf{x})$	Strain components
ε_{ij}^* (ε^*)	Uniform dilatational eigenstrains
J_I	Functions related to elliptic integrals
λ, λ^*	Largest positive root of cubic equations
λ_T	Coefficient of linear thermal expansion
ρ, ρ^*	Symbols to simplify the expression
$\sigma_{ij}(\mathbf{x})$	Stress components
σ_0	Normalized factor
μ	Shear modulus
ν	Poisson's ratio

Subscripts

i, j	Index of Cartesian component

Superscripts

ext	The exterior field
int	The interior field
(in)	Quantities just inside the inclusion
(out)	Quantities just outside the inclusion
*	Term reflecting the effects of the boundary surface
=	Indicating the solution of the dilatational inclusion in a full space

inclusion problems have a variety of significant applications in the geophysical systems, including fault zones, compaction bands and intrusions, even for the renewable and sustainable energy of geothermal reservoirs and volcanoes.

A spheroid is an ellipsoid with two equal semi-diameters, or called ellipsoid of revolution. The quadric surface of a spheroid is obtained by rotating an ellipse about one of its principal axes. To be specific, if the ellipse is rotated about its major axis, the result is a prolate (elongated) spheroid, as compared to the oblate (flattened) spheroid which is rotated about its minor axis. If the generating ellipse is a circle, the result is a sphere. Manoylov et al. (2013) demonstrated that spheroid may allow for a more versatile model than sphere for predicting the elastic characteristics porous materials. Since spheroids may represent a wide range of geometries varying from spherical to layer-like shapes, Rudnicki (1999) employed the spheroidal inclusion model to solve various geophysical problems with applications to aquifers and reservoirs by taking advantage of the handy analytical solutions available for the full space problem. However, it would be desirable to extend the spheroidal inclusion model (Rudnicki, 1999; Healy, 2009) to the half-space case so that the influences of the free surface may be more accurately evaluated. The axisymmetric problems considering vertically aligned spheroidal inclusions have been studied (Yu and Sanday, 1990; Korsunsky, 1997), while the asymmetric problems concerning horizontally aligned spheroidal inclusions have not received much attention and cannot be analytically treated by those axisymmetric approaches (Yu and Sanday, 1990; Korsunsky, 1997).

Another known issue is that the classical Eshelby solution involves derivatives of elliptic integrals of the first and second kinds, and usually cannot be expressed in closed-form with elementary function. Furthermore, in the presence of free surface, the expressions will become lengthy and difficult to manage. A semi-infinite space containing a three dimensional inclusion other than polyhedral shape can hardly be solved in closed-form. The current work is a rare exception in which a closed-form formulation does exist for a horizontally aligned thermo-porous spheroidal inclusion in a semi-infinite solid. Furthermore, the study is complementary to the axisymmetric cases investigated previously by Yu and Sanday (1990) and Korsunsky (1997). It is noted that although technically axisymmetric problem might be more interesting, these two works did not present explicit results, nor were the elastic solutions complete (i.e. in the sense of both displacement and stress). Using a geometric interpretation, the current study proposes an effective way to analytically treat the asymmetric problems. We derived complete elastic field solutions corresponding to the displacement, strain and stress for both the interior and exterior fields due to either prolate or oblate spheroid shaped inclusion in a semi-infinite space. These analytical and explicit expressions therefore attempt to overcome the mathematical difficulties due to the mirror image terms stemming from the effect of the free boundary surface. Furthermore, all the formulae derived in this paper are geometrically meaningful and are expressed in explicit closed-form.

This paper is organized as follows. The solution of an ellipsoidal inclusion with thermo-porous eigenstrains in a half-space is reviewed with geometric representation in Section 2. By employing the trigonometric and logarithmic functions, the J-function for the oblate and prolate spheroidal inclusions are represented in closed form. Based on the outward unit normal vector of an imaginary confocal ellipsoid, we present the solution for full elastic fields with respect to the displacement, strain and stress components in Section 3. For the convenience of engineering applications, the source codes programmed in FORTRAN language are detailed in Section 4. Jump conditions across the interface between the inclusion and surrounding matrix are discussed, and illustrative benchmarking examples particularly with geostructural applications involving poroelastic and thermoelastic strains are provided to validate the present solution in Section 5. The concluding remarks are presented in Section 6. The solution of the interior field with respect to the displacement, strain and stress components are listed in the Appendix for ease of reference.

2. Geometric interpretation of the solution for an ellipsoidal inclusion with dilatational eigenstrains in a half-space

Eigenstrain, ε_{ij}^*, is a generic name to represent a broad range of inelastic strains, such as thermal strains, plastic strains, phase transformation, and misfit strains (Mura, 1987). For an isotropic thermo-poroelastic solid, ε_{ij}^* due to pore-pressure and thermal expansion may be represented as (Segall and Fitzgerald, 1998)

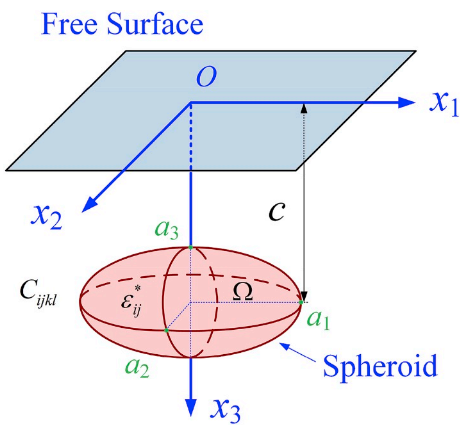

Fig. 1. Schematic illustration of a spheroidal inclusion with uniform dilatational eigenstrains in a half-space.

$$\varepsilon_{ij}^* = \frac{1-2\nu}{2\mu(1+\nu)}\delta_{ij}\alpha_B(P-P_o) + \delta_{ij}\lambda_T(T-T_o) \tag{1}$$

where P, T, P_o, T_o are pore pressure, temperature, the unstrained state of pore pressure and temperature, respectively. Moreover, α_B is the Biot pore-pressure coefficient, where $\alpha_B \approx 1$ for compliant porous matrix and $\alpha_B \approx 0$ for stiff matrix; λ_T is the coefficient of linear thermal expansion. Assuming thermo-porous eigenstrain $\varepsilon_{11}^* = \varepsilon_{22}^* = \varepsilon_{33}^* = \varepsilon^*$ and $\varepsilon_{12}^* = \varepsilon_{13}^* = \varepsilon_{23}^* = 0$ uniformly distributed within the inclusion, and vanished in the surrounding matrix.

Consider a semi-infinite matrix containing an ellipsoidal inclusion, Ω, which is defined as (Fig. 1)

$$\frac{x_1^2}{a_1^2} + \frac{x_2^2}{a_2^2} + \frac{(x_3-c)^2}{a_3^2} \le 1, \qquad (c \ge a_3) \tag{2}$$

where a_I ($I = 1, 2, 3$) is the semi-axis of the ellipsoidal inclusion with center at (0,0, c). The boundary surface, $x_3 = 0$, is free from any external tractions. For any point $\mathbf{x}(x_1, x_2, x_3)$ located outside the inclusion, a confocal imaginary ellipsoid is constructed (Fig. 2).

$$\frac{x_1^2}{a_1^2+\lambda} + \frac{x_2^2}{a_2^2+\lambda} + \frac{(x_3-c)^2}{a_3^2+\lambda} = 1 \tag{3}$$

where λ is the largest positive root of the confocal imaginary ellipsoid in Eq. (3). When a point is located inside the inclusion, the value of λ vanishes. To account for the mirrored ellipsoid, the mirrored confocal ellipsoid is constructed by passing an exterior point similar to the confocal imaginary ellipsoid and defined as

$$\frac{x_1^2}{a_1^2+\lambda^*} + \frac{x_2^2}{a_2^2+\lambda^*} + \frac{(x_3+c)^2}{a_3^2+\lambda^*} = 1 \tag{4}$$

where λ^* is the largest positive root of Eq. (4).

The displacement solution of an ellipsoidal inclusion with uniform dilatational eigenstrains in a semi-infinite space may be presented as

$$\frac{(1-\nu)u_i(\mathrm{x})}{(1+\nu)\varepsilon^*} = \begin{cases} x_i \underline{\underline{J_I(\lambda)}} + (3-4\nu)x_iJ_I(\lambda^*) - 2x_3\rho_{123}^*n_3^*n_i^*, \ (i=1,2) \\ \underline{\underline{(x_3-c)J_3(\lambda)}} + [2x_3 - (3-4\nu)(x_3+c)]J_3(\lambda^*) \\ \quad - 2x_3\rho_{123}^*n_3^{*2}, \ (i=3) \end{cases} \tag{5}$$

where ν is Poisson's ratio and the J_I−functions of elliptic integrals are detailed in our previous work (Jin et al., 2016, 2017). The terms with superscript (*) in Eq. (5) reflect the effects of the boundary surface related to the mirrored images. The double underlined terms in above equation denote the corresponding solution of an infinite extended space case in the absence of the boundary surface. The additional

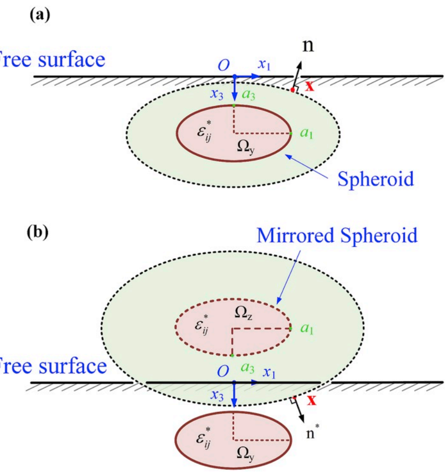

Fig. 2. Schematic of the original and mirrored ellipsoidal inclusion. For any exterior points **x** located outside the inclusion, an imaginary ellipsoid is constructed with the outward unit normal vector denoted by n (Fig. 2a); the imaginary spheroid confocal to the mirrored inclusion is constructed passing the exterior points **x**, where the corresponding outward unit normal vector is denoted by n^* (Fig. 2b).

ρ-functions are

$$\rho_{123} = \frac{a_1a_2a_3}{\sqrt{(a_1^2+\lambda)(a_2^2+\lambda)(a_3^2+\lambda)}}, \quad \rho_{123}^* = \frac{a_1a_2a_3}{\sqrt{(a_1^2+\lambda^*)(a_2^2+\lambda^*)(a_3^2+\lambda^*)}} \tag{6}$$

Ju and Sun (1999) introduced the outward unit normal vector n_i at a matrix point $\mathbf{x}(x_1, x_2, x_3)$ on the imaginary ellipsoid surface (Fig. 2). The method of Ju and Sun (1999) can be extended to a half-space inclusion problem, and the outward unit normal vectors of the imaginary confocal ellipsoids with respect to the original and mirrored ellipsoidal inclusion are denoted by n_i (Fig. 2a) and n_i^* (Fig. 2b).

$$n_i = \begin{cases} \frac{x_i}{(a_I^2+\lambda)\sqrt{H(\lambda)}}, & (i=1,2) \\ \frac{x_i-c}{(a_I^2+\lambda)\sqrt{H(\lambda)}}, & (i=3) \end{cases}, H(\lambda) = \frac{x_1^2}{(a_1^2+\lambda)^2} + \frac{x_2^2}{(a_2^2+\lambda)^2} + \frac{(x_3-c)^2}{(a_3^2+\lambda)^2} \tag{7}$$

Similarly,

$$n_i^* = \begin{cases} \frac{x_i}{(a_I^2+\lambda^*)\sqrt{H(\lambda^*)}}, & (i=1,2) \\ \frac{x_i+c}{(a_I^2+\lambda^*)\sqrt{H(\lambda^*)}}, & (i=3) \end{cases}, H(\lambda^*) = \frac{x_1^2}{(a_1^2+\lambda^*)^2} + \frac{x_2^2}{(a_2^2+\lambda^*)^2} + \frac{(x_3+c)^2}{(a_3^2+\lambda^*)^2} \tag{8}$$

Subsequently, the strain components may be obtained by differentiating the displacement solution of Eq. (5), and the stresses are determined through Hooke's law. Noting that the value of λ and the J_I-function cannot be expressed in closed-form with elementary functions.

3. The closed-form solution to the spheroidal inclusion with dilatational eigenstrains

3.1. Simplification for the spheroidal inclusion

Although geostructures may seldom be of exactly spheroidal shape, this geometry encompasses a wide range of possible shapes, and is frequently a good approximation. Unlike a general ellipsoid, the value of λ, J_1-functions and outward unit normal vectors of the spheroidal shape can be derived in closed-form with only elementary functions. The solution for the case of a spheroidal inclusion may be derived from Section 2 by setting $a_1 \neq a_2 = a_3$, and consequently the value of λ for the exterior field is

$$\lambda = \frac{1}{2}[x_1^2 + x_2^2 + (x_3 - c)^2 - a_1^2 - a_3^2] + \sqrt{\frac{1}{4}[x_1^2 + x_2^2 + (x_3 - c)^2 + a_1^2 - a_3^2]^2 + (a_3^2 - a_1^2)x_1^2} \tag{9}$$

For the degenerate case of a spherical inclusion ($a_1 = a_2 = a_3 = a$), the corresponding value of λ may be written as

$$\lambda = x_1^2 + x_2^2 + (x_3 - c)^2 - a^2 \tag{10}$$

By setting $\alpha \equiv \frac{a_1}{a_3}$, the corresponding J_1-functions for the oblate spheroidal inclusion ($a_1 < a_2 = a_3$) and prolate spheroidal inclusion ($a_1 > a_2 = a_3$) in the exterior field may be expressed in terms of elementary functions

$$J_1 = \begin{cases} \frac{\alpha}{(1-\alpha^2)^{\frac{3}{2}}}(\tan\beta - \beta), & \beta = \arccos\sqrt{\frac{a_1^2+\lambda}{a_3^2+\lambda}}, \ (\text{for } \alpha < 1) \\ \frac{\alpha}{(\alpha^2-1)^{\frac{3}{2}}}\left[-\ln\left(\tan\frac{\gamma}{2}\right) - \cos\gamma\right], & \gamma = \arcsin\sqrt{\frac{a_3^2+\lambda}{a_1^2+\lambda}}, \ (\text{for } \alpha > 1) \end{cases} \tag{11}$$

The J_1-function for a spherical inclusion ($a_1 = a_2 = a_3 = a$, or $\alpha = 1$) may be deduced by employing the L'hospital rule

$$J_1 = \frac{a^3}{3(a^2 + \lambda)^{\frac{3}{2}}} \tag{12}$$

3.2. The complete elastic field of spheroidal inclusion with dilatational eigenstrains

The solution to a spheroidal inclusion with dilatational eigenstrains in a semi-infinite medium may be presented in explicit closed-form. The displacement solution in exterior field may be derived as

$$u_i(\mathrm{x}) = \frac{1+\nu}{1-\nu}W_i(\mathrm{x})\varepsilon^* \tag{13}$$

wherein

$$W_1(\mathrm{x}) = x_1 J_1(\lambda) + (3-4\nu)x_1 J_1(\lambda^*) - 2x_3\rho_{133}^* n_1^* n_3^* \tag{14}$$

$$W_2(\mathrm{x}) = \frac{x_2}{2}[\rho_{133} - J_1(\lambda)] + \left(\frac{3}{2} - 2\nu\right)x_2[\rho_{133}^* - J_1(\lambda^*)] - 2x_3\rho_{133}^* n_2^* n_3^* \tag{15}$$

$$W_3(\mathrm{x}) = \frac{x_3 - c}{2}[\rho_{133} - J_1(\lambda)] + \left[x_3 + \left(2\nu - \frac{3}{2}\right)(x_3 + c)\right][\rho_{133}^* - J_1(\lambda^*)] - 2x_3\rho_{133}^* n_3^* n_3^* \tag{16}$$

Note that for a spheroid, ρ_{123} and ρ_{123}^* in Eq. (6) are respectively renamed as ρ_{133} and ρ_{133}^*, indicating the differences between ellipsoidal and spheroidal shape:

$$\rho_{133} = \frac{a_1 a_3^2}{(a_3^2 + \lambda)\sqrt{a_1^2 + \lambda}}, \quad \rho_{133}^* = \frac{a_1 a_3^2}{(a_3^2 + \lambda^*)\sqrt{a_1^2 + \lambda^*}} \tag{17}$$

The strain solution for any exterior points may be derived as

$$\varepsilon_{ij}(\mathrm{x}) = \frac{1+\nu}{1-\nu}S_{ij}(\mathrm{x})\varepsilon^* \tag{18}$$

where

$$S_{11}(\mathbf{x}) = J_1(\lambda) - \rho_{133}n_1n_1 + (3-4\nu)[J_1(\lambda^*) - \rho_{133}^* n_1^* n_1^*] + 2\rho_{133}^* Q_{11}(\lambda^*) \tag{19}$$

$$S_{22}(\mathbf{x}) = \frac{1}{2}[\rho_{133} - J_1(\lambda)] - \rho_{133}n_2n_2 + \left(\frac{3}{2} - 2\nu\right)[\rho_{133}^* - J_1(\lambda^*)] + \rho_{133}^*[(4\nu - 3)n_2^* n_2^* + 2Q_{22}(\lambda^*)] \tag{20}$$

$$S_{33}(\mathbf{x}) = \frac{1}{2}[\rho_{133} - J_1(\lambda)] - \rho_{133}n_3n_3 + \left(2\nu - \frac{1}{2}\right)[\rho_{133}^* - J_1(\lambda^*)] + \rho_{133}^*[(-3 - 4\nu)n_3^* n_3^* + 2Q_{33}(\lambda^*)] \tag{21}$$

$$S_{23}(\mathbf{x}) = \underline{\underline{-\rho_{133}n_2n_3}} + \rho_{133}^*[-3n_2^* n_3^* + 2Q_{23}(\lambda^*)] \tag{22}$$

$$S_{31}(\mathbf{x}) = \underline{\underline{-\rho_{133}n_1n_3}} + \rho_{133}^*[-3n_1^* n_3^* + 2Q_{31}(\lambda^*)] \tag{23}$$

$$S_{12}(\mathbf{x}) = \underline{\underline{-\rho_{133}n_1n_2}} + \rho_{133}^*[(4\nu - 3)n_1^* n_2^* + 2Q_{12}(\lambda^*)] \tag{24}$$

where the additional Q-functions are

$$\begin{cases} Q_{11}(\lambda^*) = \frac{x_3 n_3^*}{\sqrt{H(\lambda^*)}}\left[\frac{(5-4n_1^{*2})n_1^{*2}-1}{a_1^2+\lambda^*} + \frac{4n_1^{*4}}{a_3^2+\lambda^*}\right] \\ Q_{22}(\lambda^*) = \frac{x_3 n_3^*}{\sqrt{H(\lambda^*)}}\left[\frac{(1-4n_1^{*2})n_2^{*2}}{a_1^2+\lambda^*} + \frac{4(1+n_1^{*2})n_2^{*2}-1}{a_3^2+\lambda^*}\right] \\ Q_{33}(\lambda^*) = \frac{n_3^*}{\sqrt{H(\lambda^*)}}\left[\frac{(1-4n_1^{*2})x_3 n_3^{*2}}{a_1^2+\lambda^*} + \frac{2c - x_3 + 4(1+n_1^{*2})x_3 n_3^{*2}}{a_3^2+\lambda^*}\right] \\ Q_{23}(\lambda^*) = \frac{n_2^*}{\sqrt{H(\lambda^*)}}\left[\frac{(1-4n_1^{*2})x_3 n_3^{*2}}{a_1^2+\lambda^*} + \frac{4(1+n_1^{*2})x_3 n_3^{*2}+c}{a_3^2+\lambda^*}\right] \\ Q_{31}(\lambda^*) = \frac{n_1^*}{\sqrt{H(\lambda^*)}}\left[\frac{(3-4n_1^{*2})x_3 n_3^{*2}}{a_1^2+\lambda^*} + \frac{2(1+2n_1^{*2})x_3 n_3^{*2}+c}{a_3^2+\lambda^*}\right] \\ Q_{12}(\lambda^*) = \frac{x_3 n_1^* n_2^* n_3^*}{\sqrt{H(\lambda^*)}}\left[\frac{3-4n_1^{*2}}{a_1^2+\lambda^*} + \frac{2+4n_1^{*2}}{a_3^2+\lambda^*}\right] \end{cases} \tag{25}$$

Furthermore, the solution to the exterior stress are obtained by employing Hooke's law

$$\sigma_{ij}^{ext}(\mathrm{x}) = \frac{2\mu(1+\nu)}{1-\nu}T_{ij}(\mathrm{x})\varepsilon^* \tag{26}$$

in which

$$T_{11}(\mathbf{x}) = J_1(\lambda) - \rho_{133}n_1n_1 + (3-2\nu)J_1(\lambda^*) + \rho_{133}^*[2\nu - 3n_1^* n_1^* - 4\nu n_2^* n_2^* + 2Q_{11}(\lambda^*)] \tag{27}$$

$$T_{22}(\mathbf{x}) = \frac{1}{2}[\rho_{133} - J_1(\lambda)] - \rho_{133}n_2n_2 + \left(\frac{3}{2} - 4\nu\right)[\rho_{133}^* - J_1(\lambda^*)] + \rho_{133}^*[4\nu - 3n_2^* n_2^* - 4\nu n_1^* n_1^* + 2Q_{22}(\lambda^*)] \tag{28}$$

$$T_{33}(\mathbf{x}) = \frac{1}{2}[\rho_{133} - J_1(\lambda)] - \rho_{133}n_3n_3 - \frac{1}{2}[\rho_{133}^* - J_1(\lambda^*)] + \rho_{133}^*[-3n_3^* n_3^* + 2Q_{33}(\lambda^*)] \tag{29}$$

$$T_{23}(\mathbf{x}) = S_{23}(\mathbf{x}),\ T_{31}(\mathbf{x}) = S_{31}(\mathbf{x}),\ T_{12}(\mathbf{x}) = S_{12}(\mathbf{x}) \tag{30}$$

where μ is the shear modulus and the Q-functions are presented in Eq. (25). It is noted that $T_{23}(\mathbf{x})$, $T_{31}(\mathbf{x})$ and $T_{12}(\mathbf{x})$ share the same expression with $S_{23}(\mathbf{x})$, $S_{31}(\mathbf{x})$ and $S_{12}(\mathbf{x})$ for the exterior field. The corresponding results of the displacement, strain and stress for the interior field are listed in the Appendix.

4. Implementation

The FORTRAN package of this paper is provided with multiple files, which are convenient for user to download and calculate the complete elastic fields, corresponding to the displacement, strain and stress, produced by a horizontally aligned spheroidal inclusion with uniform dilatational eigenstrains in a half-space. The current formulae are

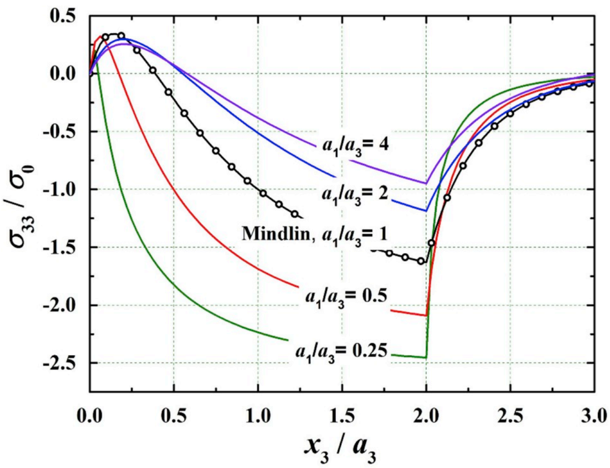

Fig. 3. Benchmark example.

implemented in matrix form (Jin et al., 2011, 2014), and the Voigt notation is employed for ease of programming. The description of the present code is detailed as follows.

(1) **Main.f90** contains the codes **CPDISP**, **CPSTRN** and **CPSTR** to calculate the elastic fields with respect to the displacement, strain and stress of the spheroidal inclusion, respectively. The solution for points on the interface is evaluated in **CPINTERFACE.** In order to validate the presented solution, extensive benchmarks are studied and dimensionless results of full field for the spheroidal inclusion are reported in this project.

(2) **Functions.f90** constructs the basic functions, which are frequently used in determining the displacement, strain and stress components. Subroutine **LMDSPH** is used to obtain the closed-form value of λ for either oblate, prolate spheroidal or spherical inclusion. **RLROOTEX** determines the values of λ^* and λ outside the original ellipsoidal inclusion, while **RLROOTIN** calculates the λ^* inside the original ellipsoid, noting that λ vanishes inside the original ellipsoidal inclusion. Moreover, **TERMH** represents the terms $H(\lambda)$, $H(\lambda^*)$ in Eqs. (7) and (8), **UNITVECT** shows the outward unit normal vector, n_i, n_i^*, of the imaginary confocal ellipsoids with respect to the original and mirrored ellipsoidal inclusion in Eqs. (7) and (8). Note that the subroutine **UNITVECT** also evaluates ρ_{133} and ρ_{133}^* in Eq. (17). Subroutine **J1FUN** exhibits the closed-form of J_1-function for the oblate, prolate spheroidal and spherical inclusions, cf. Eqs. (11) and (12).

(3) **Displacement.f90** calculates the displacements for the exterior and interior fields. **HFDSPCOF** checks the target points' location. Subroutines **UIEXCOFF** and **EXDISP3** respectively determine the coefficients and solution of the displacement for exterior points using Eqs. (13)–(16), while **UIINCOFF** and **INDISP3** evaluate the counterparts for interior points according to Eq. (A1)-(A4).

(4) **Strain.f90** determines the strain components for the exterior and interior fields. **HFSTNCOF** checks the points' location in the exterior or interior field. For exterior points, the influence coefficients of the strains, cf. Eqs. (19)–(24), are evaluated in Subroutine EIJEXCOFF, which are then called by **EXSTRN6** to determine the strain components produced by the thermal inclusion. The term Q-functions in Eq. (25) are programmed in **TERMQIJZ.** In parallel, the corresponding subroutines for evaluating the interior strain field utilizes **EIJINCOFF** and **INSTRN6** according to Eq. (A5)-(A11).

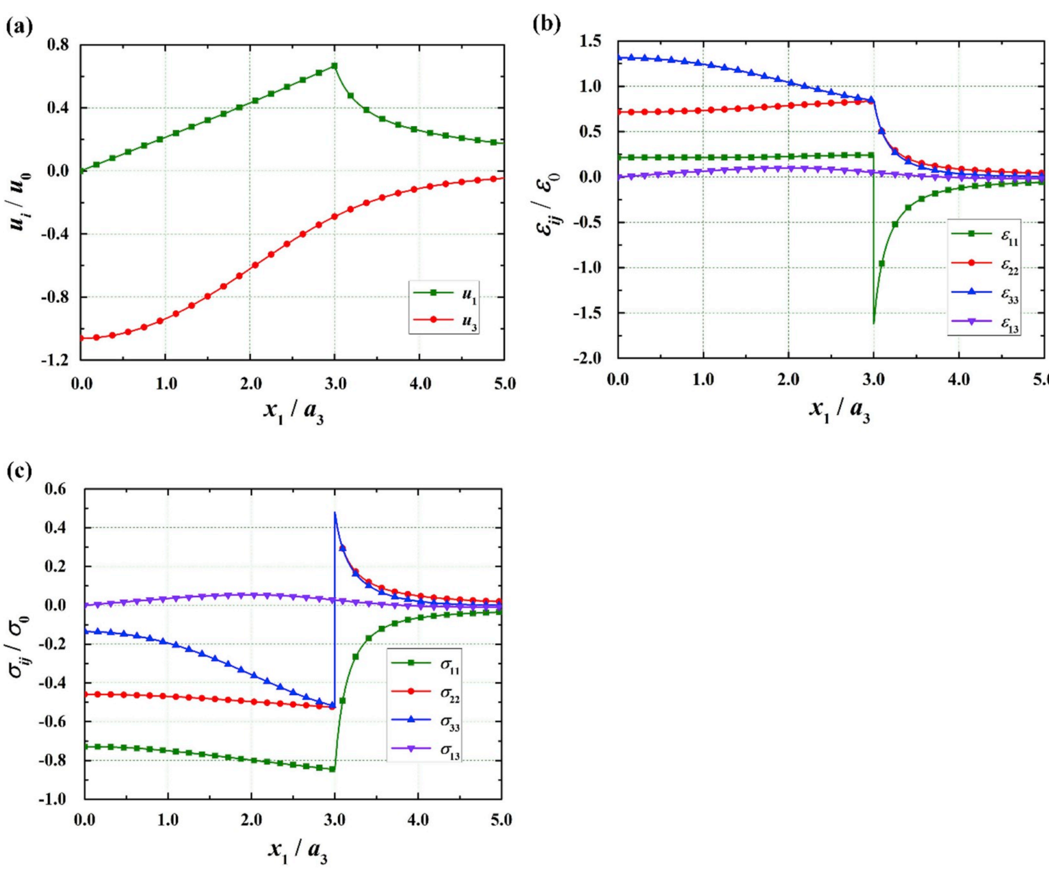

Fig. 4. Dimensionless results for the prolate spheroidal inclusion with thermal eigenstrains are compared along the x_1-direction: (a) variation of displacements; (b) variation of strains; (c) variation of stresses.

(5) **Stress.f90** constructs the solution for the exterior and interior stress components. **HFSTRCOE** checks the points' location. The subroutine **SIJEXCOFF** determines the influence coefficients and is subsequently called by **STREXFLD** to solve the exterior stress field, cf. Eqs. (26)–(30). Furthermore, **SIJINCOFF** and **STRINFLD** are programmed according to Eq. (A12)-(A16), which present the solution for the interior stress field.

5. Discussions

For the interior field, the formulae of the displacement and strain are identical with the expressions of the corresponding exterior field, but the parameter $\lambda = 0$ and the parts containing the outward unit normal vector n_i vanish. To be specific, the double underlined terms of the displacement in Eqs. (14)–(16) are replaced by $y_1 J_1(0)$, $\frac{y_i}{2}[1 - J_1(0)]$, and the strain components in Eqs. (19)–(21) are replaced by $J_1(0)$, $\frac{1}{2}[1 - J_1(0)]$, respectively. However, the double underlined terms of the stress components in Eqs. (27)–(29) become $J_1(0) - 1$, $-\frac{1}{2}[1 + J_1(0)]$. For convenience of reference, the interior solutions are given in the Appendix.

5.1. Interface discontinuity

It is of interest to examine the jump conditions of the displacements, strains and stresses between the inclusion and the surrounding matrix. The jump of displacements is determined as

$$\Delta u_i(\mathbf{x}) = u_i^{(\mathrm{out})}(\mathbf{x}) - u_i^{(\mathrm{in})}(\mathbf{x}) = \frac{1+\nu}{1-\nu}\Delta W_i(\mathbf{x})\varepsilon^* \tag{31}$$

where the superscripts (out) and (in) respectively represent quantities just outside and just inside the inclusion. When the target points move to the interface either from the inside or outside of the inclusion, the term $\rho_{13}(0) = 1$. This result immediately verifies the displacement across the interface between the inclusion and the surrounding matrix must be continuous:

$$\Delta W_i(\mathbf{x}) = W_i(\mathbf{x}) - w_i(\mathbf{x}) = 0 \tag{32}$$

The jump of the strains across the interface are found to be

$$\Delta\varepsilon_{ij}(\mathrm{x}) = \varepsilon_{ij}^{(out)}(\mathrm{x}) - \varepsilon_{ij}^{(in)}(\mathrm{x}) = \frac{1+\nu}{1-\nu}\Delta S_{ij}(\mathrm{x})\varepsilon^* \tag{33}$$

in which

$$\Delta S_{ij}(\mathrm{x}) = S_{ij}(\mathrm{x}) - s_{ij}(\mathrm{x}) = -n_i n_j \tag{34}$$

For instance

$$\Delta S_{11}(\mathrm{x}) = -n_1 n_1,\ \Delta S_{33}(\mathrm{x}) = -n_3 n_3,$$
$$\Delta S_{13}(\mathrm{x}) = -n_1 n_3 \tag{35}$$

The jump of the corresponding stresses may be denoted as

$$\Delta\sigma_{ij}(\mathrm{x}) = \sigma_{ij}^{(out)}(\mathrm{x}) - \sigma_{ij}^{(in)}(\mathrm{x}) = \frac{2\mu(1+\nu)}{1-\nu}\Delta T_{ij}(\mathrm{x})\varepsilon^* \tag{36}$$

wherein

$$\Delta T_{ij}(\mathrm{x}) = T_{ij}(\mathrm{x}) - t_{ij}(\mathrm{x}) = \delta_{ij} - n_i n_j \tag{37}$$

That is, for example

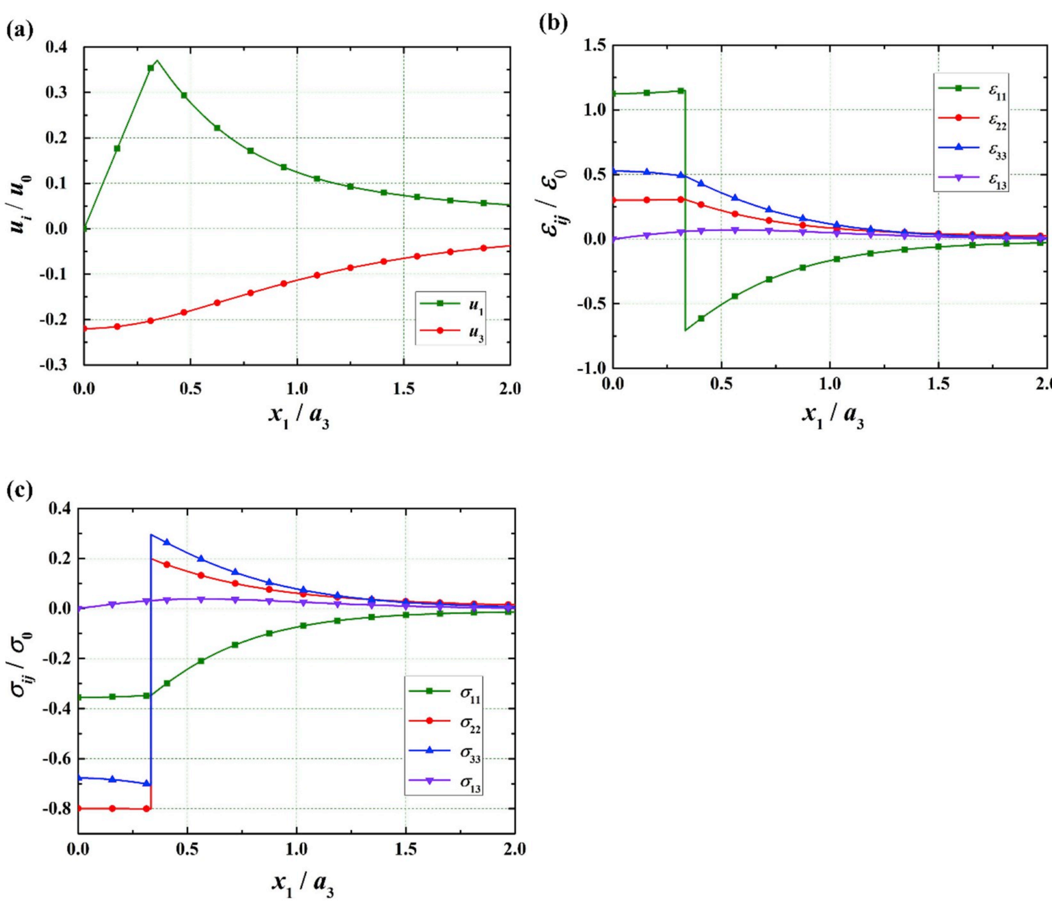

Fig. 5. Dimensionless results for the oblate spheroidal inclusion with thermal eigenstrains are compared along the x_1-direction: (a) variation of displacements; (b) variation of strains; (c) variation of stresses.

$$\Delta T_{11}(\mathrm{x}) = 1 - n_1 n_1,\ \Delta T_{33}(\mathrm{x}) = 1 - n_3 n_3,$$
$$\Delta T_{13}(\mathrm{x}) = -n_1 n_3 \tag{38}$$

Similarly, other entries of Eqs. (35) and (38) may be obtained by the cyclic permutation with respect to subindices (1, 2, 3).

5.2. Benchmark examples

In order to compare the results with the known solution by Mindlin and Mura, analytical calculations are carried out with $\nu = 0.3$. The shape effect of the inclusion on the stress σ_{33}, which is normalized by $\sigma_0 = E\lambda_T \Delta T/3(1-\nu)$, is plotted along the x_3-direction at a depth of $c = a_3$ in Fig. 3. In the calculation, the aspect ratio of a_1/a_3 ranges from 0.25 to 4 and the special case of spherical inclusion ($a_1/a_3 = 1$) may serve as a benchmark example to validate the present closed-form solution. When a spheroid transforms into a sphere, the result exactly reproduces Mindlin and Cheng's solution (1950). For the spheroidal inclusion ($a_1/a_3 = 0.25$), the compressive stress component σ_{33} shows larger value as compared to that of other shaped spheroids when $x_3/a_3 < 2$. However, the stress components for the five types of spheroids decrease to zero after the points are far from $x_3/a_3 = 3$. It can be concluded that the stress distributions are apparently influenced by the free boundary surface and the shape of the inclusion.

Seo and Mura (1979) reports the axisymmetric problems of vertically placed spheroidal inclusions, while the problem concerning horizontally aligned spheroidal inclusions is given in this section. The prolate spheroidal ($a_1 = 3a_2 = 3a_3$) and oblate spheroidal ($3a_1 = a_2 = a_3$) inclusions with thermal eigenstrains are reported according to the current solution. The displacements, strains, and stresses for the prolate and oblate spheroidal inclusions along the x_1-direction with at depth $c = a_3$ are shown in Figs. 4 and 5, respectively. The displacements, strains and stress components are normalized by $u_0 = \lambda_T \Delta T a_3$, $\varepsilon_0 = \lambda_T \Delta T$ and $\sigma_0 = E\lambda_T \Delta T/(1-\nu)$, respectively. The stresses and strains for the interior field are no longer constant due to the existence of the free surface, as opposed to the inclusion in a full-space. The stresses and strains become almost zero for $x_1/a_3 = 5$ which pertains to the prolate spheroidal case, as compared to the oblate spheroidal case with stress and strain components approaching to zero in the limit $x_1/a_3 = 2$. The present plots verify that the strain and stress fields suffer discontinuities across the interface between the inclusion and the surrounding matrix, while the displacements are continuous across the boundary of the inclusion.

The results for the elastic field due to the fluid withdrawal leading to the pore pressure are analyzed and the corresponding displacements, strains and stresses are shown in Fig. 6 (prolate spheroid) and Fig. 7 (oblate spheroid). The displacements, strains and stress components are normalized by setting $u_0 = -(1-2\nu)\alpha P/Ea_3$, $\varepsilon_0 = -(1-2\nu)\alpha P/E$ and $\sigma_0 = -\alpha P$, respectively The displacement u_1 is negative inside the inclusion and approaches zero for $x_1/a_3 > 5$ of the prolate spheroid, as compared to the oblate spheroidal case with a displacement approaching zero for the condition $x_1/a_3 > 2$. Moreover, the strain component ε_{11} represents compression inside the inclusion and which converts to tension in the surrounding matrix, while the other strain components are always in a compressive state and that increases with x_1/a_3. The stress σ_{33} inside the inclusion can have a tension region, and jumps to compression in the matrix.

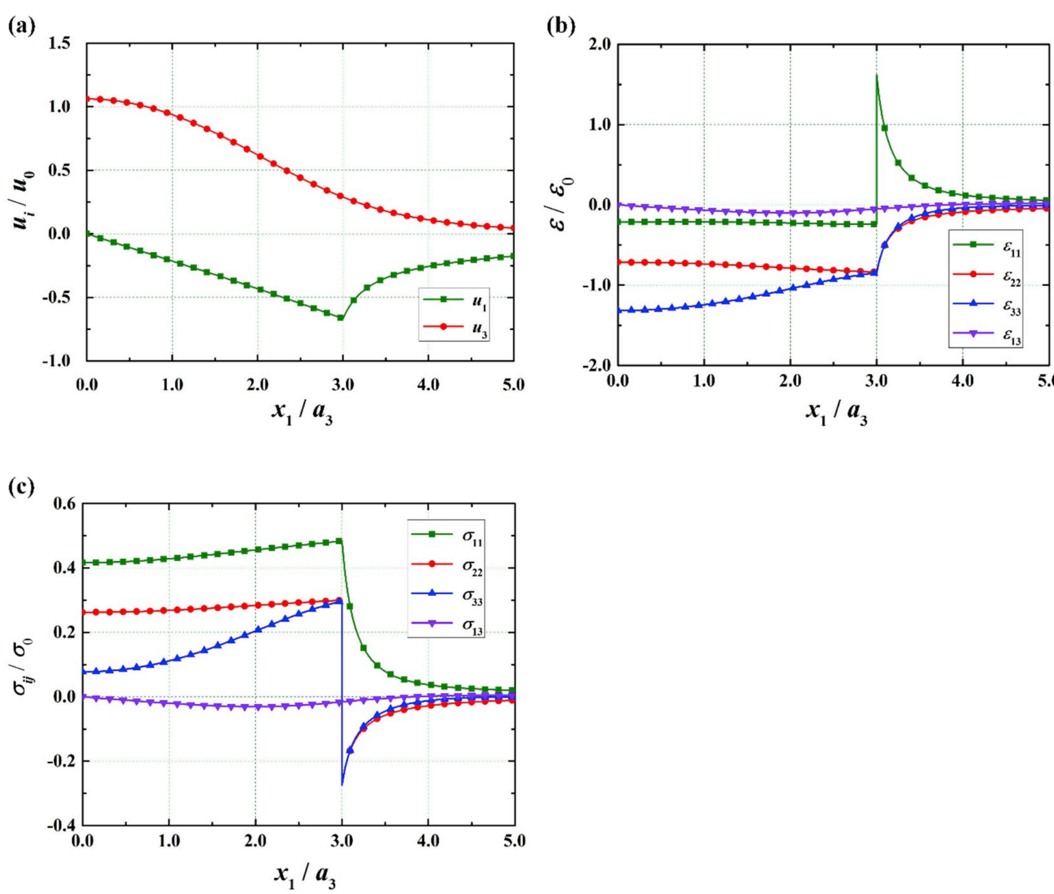

Fig. 6. Dimensionless results for the prolate spheroidal inclusion with porous eigenstrains are compared along the x_1-direction: (a) variation of displacements; (b) variation of strains; (c) variation of stresses.

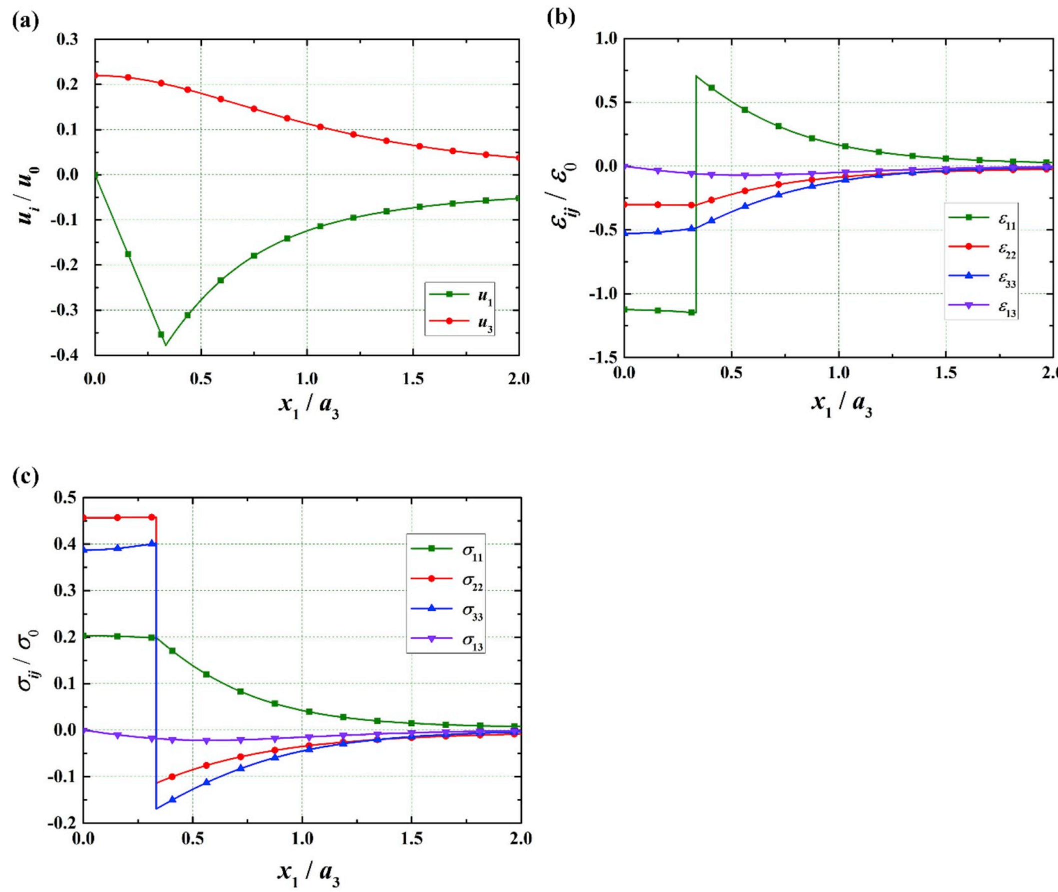

Fig. 7. Dimensionless results for the oblate spheroidal inclusion with porous eigenstrains are compared along the x_1-direction: (a) variation of displacements; (b) variation of strains; (c) variation of stresses.

6. Concluding remarks

The inclusion problems for determining the elastic field around the inhomogeneities have wide applications in the field of geophysics. The exterior field of a spheroidal inclusion in a half-space tends to be more complex and intricate. For the case of spheroidal inclusion with pure dilatational eigenstrains, the obstacle may be conquered by introducing the outward unit normal vector of an imaginary confocal ellipsoid and the closed-form of J_1-function for the oblate and prolate spheroidal shape both in a full-space and a half-space is obtained by adopting the trigonometric and logarithmic functions. Thus, a complete solution with respect to the displacement, strain and stress may be derived in a compact and explicit closed-form.

In conjunction with interior field solution (given in the Appendix), the full field closed-form solution can be utilized to predict the localized heating due to temperature changes, or pressure alterations caused by fluid mass injection or withdrawal for the geothermal reservoirs. The double underlined terms in the expressions denote the corresponding solution for an infinitely extended medium. The discontinuities across the interface between the inclusion and surrounding matrix are related only to the underlined terms and are identical to those of a full-space. We also developed a FORTRAN code to calculate the elastic field of the oblate and prolate spheroidal inclusion produced by uniform dilatational eigenstrains in a semi-infinite solid. In addition, illustrative benchmark examples are provided to validate the present analytical solution and the source code can be downloaded from the journal website for the convenience of engineering applications in the field of geophysics.

Acknowledgement

This work is supported by the National Natural Science Foundation of China (Grant Nos. 51475057 and 51875059). X.Z. and P.L. are grateful to the Graduate Research and Innovation Foundation of Chongqing, China (Grant Nos. CYB17025 and CYB18020). X.J. would also like to acknowledge the support from Fundamental Research Funds for the Central Universities (Nos.106112017CDJQJ328839 and 2018CDYJSY0055), and the State Key Laboratory of Mechanical Transmissions through funding (SKLMT-ZZKT-2017M15). X.Z. and X.J. want to extend a special thanks to Dr. Jamieson Brechtl for his helpful discussion and support.

Appendix A. Supplementary data

Supplementary data to this article can be found online at https://doi.org/10.1016/j.cageo.2018.10.001.

Appendix. Interior field solution

For any interior points, the elastic solution to the displacement, strain and stress components are obtained by setting $\lambda = 0$, $n_i = 0$, $\rho_{133} = 1$. Hence, from Eqs. (13)–(17), the displacements for interior points may be obtained as

$$u_i(\mathrm{x}) = \frac{1+\nu}{1-\nu} w_i(\mathrm{x})\varepsilon^* \tag{A1}$$

where

$$w_1(\mathbf{x}) = x_1 J_1(0) + (3-4\nu)x_1 J_1(\lambda^*) - 2x_3\rho_{133}^* n_1^* n_3^* \tag{A2}$$

$$w_2(\mathrm{x}) = \frac{x_2}{2}[1 - J_1(0)] + \left(\frac{3}{2} - 2\nu\right)x_2[\rho_{133}^* - J_1(\lambda^*)] - 2x_3\rho_{133}^* n_2^* n_3^* \tag{A3}$$

$$w_3(\mathrm{x}) = \frac{x_3 - c}{2}[1 - J_1(0)] + \left[x_3 + \left(2\nu - \frac{3}{2}\right)(x_3 + c)\right][\rho_{133}^* - J_1(\lambda^*)] - 2x_3\rho_{133}^* n_3^* n_3^* \tag{A4}$$

The closed-form solution for the interior strain field is determined in view of Eq. (18)

$$\varepsilon_{ij}(\mathrm{x}) = \frac{1+\nu}{1-\nu} s_{ij}(\mathrm{x})\varepsilon^* \tag{A5}$$

To be specific,

$$s_{11}(\mathbf{x}) = J_1(0) + (3-4\nu)[J_1(\lambda^*) - \rho_{133}^* n_1^* n_1^*] + 2\rho_{133}^* Q_{11}(\lambda^*) \tag{A6}$$

$$s_{22}(\mathbf{x}) = \frac{1}{2}[1 - J_1(0)] + \left(\frac{3}{2} - 2\nu\right)[\rho_{133}^* - J_1(\lambda^*)] + \rho_{133}^*[(4\nu - 3)n_2^* n_2^* + 2Q_{22}(\lambda^*)] \tag{A7}$$

$$s_{33}(\mathbf{x}) = \frac{1}{2}[1 - J_1(0)] + \left(2\nu - \frac{1}{2}\right)[\rho_{133}^* - J_1(\lambda^*)] + \rho_{133}^*[(-3 - 4\nu)n_3^* n_3^* + 2Q_{33}(\lambda^*)] \tag{A8}$$

$$s_{23}(\mathbf{x}) = \rho_{133}^*[-3n_2^* n_3^* + 2Q_{23}(\lambda^*)] \tag{A9}$$

$$s_{31}(\mathbf{x}) = \rho_{133}^*[-3n_1^* n_3^* + 2Q_{31}(\lambda^*)] \tag{A10}$$

$$s_{12}(\mathbf{x}) = \rho_{133}^*[(4\nu - 3)n_1^* n_2^* + 2Q_{12}(\lambda^*)] \tag{A11}$$

From the aforementioned expression of Eq. (26) with respect to the exterior stress field, the corresponding stress solution for interior points may be presented as

$$\sigma_{ij}^{\mathrm{int}}(\mathrm{x}) = \frac{2\mu(1+\nu)}{1-\nu} t_{ij}(\mathrm{x})\varepsilon^* \tag{A12}$$

wherein

$$t_{11}(\mathbf{x}) = J_1(0) - 1 + (3-2\nu)J_1(\lambda^*) + \rho_{133}^*[2\nu - 3n_1^* n_1^* - 4\nu n_2^* n_2^* + 2Q_{11}(\lambda^*)] \tag{A13}$$

$$t_{22}(\mathbf{x}) = -\frac{1}{2} - \frac{1}{2}J_1(0) - \left(\frac{3}{2} - 4\nu\right)J_1(\lambda^*) + \rho_{133}^*\left[\frac{3}{2} - 3n_2^* n_2^* - 4\nu n_1^* n_1^* + 2Q_{22}(\lambda^*)\right] \tag{A14}$$

$$t_{33}(\mathbf{x}) = -\frac{1}{2} - \frac{1}{2}J_1(0) + \frac{1}{2}J_1(\lambda^*) + \rho_{133}^*\left[-\frac{1}{2} - 3n_3^* n_3^* + 2Q_{33}(\lambda^*)\right] \tag{A15}$$

$$t_{23}(\mathbf{x}) = s_{23}(\mathbf{x}), \quad t_{31}(\mathbf{x}) = s_{31}(\mathbf{x}), \quad t_{12}(\mathbf{x}) = s_{12}(\mathbf{x}) \tag{A16}$$

where the Q-functions are given in Eq. (25)

References

Bedayat, H., Dahi Taleghani, A., 2015. Two interacting ellipsoidal inhomogeneities: applications in geoscience. Comput. Geosci. 76, 72–79.
Chiu, Y.P., 1978. On the stress field and surface deformation in a half space with a cuboidal zone in which initial strains are uniform. J. Appl. Mech. 45, 302–306.
Eshelby, J.D., 1957. The determination of the elastic field of an ellipsoidal inclusion, and related problems. Proc. Roy. Soc. Lond. Math. Phys. Sci. 241, 376–396.
Eshelby, J.D., 1959. The elastic field outside an ellipsoidal inclusion. Proc. Roy. Soc. Lond. Math. Phys. Sci. 252, 561–569.
Healy, D., 2009. Elastic field in 3D due to a spheroidal inclusion—MATLAB™ code for Eshelby's solution. Comput. Geosci. 35, 2170–2173.
Im, K., Elsworth, D., Guglielmi, Y., Mattioli, G.S., 2017. Geodetic imaging of thermal deformation in geothermal reservoirs - production, depletion and fault reactivation. J. Volcanol. Geoth. Res. 338, 79–91.

Jin, X., Keer, L.M., Wang, Q., 2011. A closed-form solution for the Eshelby tensor and the elastic field outside an elliptic cylindrical inclusion. J. Appl. Mech. 78, 031009.
Jin, X., Wang, Z., Zhou, Q., Keer, L.M., Wang, Q., 2014. On the solution of an elliptical inhomogeneity in plane elasticity by the equivalent inclusion method. J. Elasticity 114, 1–18.
Jin, X., Lyu, D., Zhang, X., Zhou, Q., Wang, Q., Keer, L.M., 2016. Explicit analytical solutions for a complete set of the Eshelby tensors of an ellipsoidal inclusion. J. Appl. Mech. 83, 121010–121012.
Jin, X., Zhang, X., Li, P., Xu, Z., Hu, Y., Keer, L.M., 2017. On the displacement of a two-dimensional Eshelby inclusion of elliptic cylindrical shape. J. Appl. Mech. 84, 074501–074506.
Ju, J.W., Sun, L.Z., 1999. A novel formulation for the exterior-point eshelby's tensor of an ellipsoidal inclusion. J. Appl. Mech. 66, 570–574.
Korsunsky, A.M., 1997. An axisymmetric inclusion in one of two perfectly bonded dissimilar elastic half-spaces. J. Appl. Mech. 64, 697–700.
Liu, S., Jin, X., Wang, Z., Keer, L.M., Wang, Q., 2012. Analytical solution for elastic fields caused by eigenstrains in a half-space and numerical implementation based on FFT. Int. J. Plast. 35, 135–154.
Lyu, D., Zhang, X., Li, P., Luo, D., Hu, Y., Jin, X., Zhang, L., Keer, L.M., 2018. Explicit analytical solutions for the complete elastic field produced by an ellipsoidal thermal inclusion in a semi-infinite space. J. Appl. Mech. 85, 051005–051008.
Manoylov, A., Borodich, F.M., Evans, H.P., 2013. Modelling of elastic properties of sintered porous materials. In: Proceedings of the Royal Society of London A: Mathematical, Physical and Engineering Sciences. The Royal Society, pp. 20120689.
Meng, C., Heltsley, W., Pollard, D.D., 2012. Evaluation of the Eshelby solution for the ellipsoidal inclusion and heterogeneity. Comput. Geosci. 40, 40–48.
Mindlin, R.D., Cheng, D.H., 1950. Thermoelastic stress in the semi-infinite solid. J. Appl. Phys. 21, 931–933.
Mura, T., 1987. Micromechanics of Defects in Solids, second ed. Springer, Dordrecht, The Netherlands.
Rudnicki, J.W., 1999. Alteration of regional stress by reservoirs and other inhomogeneities: stabilizing or destabilizing? In: 9th ISRM Congress. International Society for Rock Mechanics and Rock Engineering, Paris, France.
Rudnicki, J.W., 2011. Eshelby's technique for analyzing inhomogeneities in geomechanics. In: Leroy, Y.M., Lehner, F.K. (Eds.), Mechanics of Crustal Rocks. Springer Vienna, Vienna, pp. 43–72.
Segall, P., Fitzgerald, S.D., 1998. A note on induced stress changes in hydrocarbon and geothermal reservoirs. Tectonophysics 289, 117–128.
Seo, K., Mura, T., 1979. The elastic field in a half space due to ellipsoidal inclusions with uniform dilatational eigenstrains. J. Appl. Mech. 46, 568–572.
Soltanzadeh, H., Hawkes, C.D., 2008. Semi-analytical models for stress change and fault reactivation induced by reservoir production and injection. J. Petrol. Sci. Eng. 60, 71–85.
Yu, H.Y., Sanday, S.C., 1990. Axisymmetric inclusion in a half space. J. Appl. Mech. 57, 74–77.